The Journal of Immunology

NK Cell Responses in Zika Virus Infection Are Biased towards Cytokine-Mediated Effector Functions

Christopher Maucourant, Gabriel Andrade Nonato Queiroz, Aurelien Corneau, Luana Leandro Gois, Aida Meghraoui-Kheddar, Nadine Tarantino, Antonio Carlos Bandeira, Assia Samri, Catherine Blanc, Hans Yssel, Maria Fernanda Rios Grassi and Vincent Vieillard

J Immunol 2021; 207:1333-1343; Prepublished online 18 August 2021;
doi: 10.4049/jimmunol.2001180
http://www.jimmunol.org/content/207/5/1333

The Journal of Immunology is published twice each month by
The American Association of Immunologists, Inc.,
1451 Rockville Pike, Suite 650, Rockville, MD 20852

Print ISSN: 0022-1767 Online ISSN: 1550-6606.

NK Cell Responses in Zika Virus Infection Are Biased towards Cytokine-Mediated Effector Functions

Christopher Maucourant,*[,1] Gabriel Andrade Nonato Queiroz,[†,‡,1] Aurelien Corneau,[§,1] Luana Leandro Gois,[†,‡] Aida Meghraoui-Kheddar,*[,2] Nadine Tarantino,* Antonio Carlos Bandeira,[†,¶] Assia Samri,* Catherine Blanc,[§] Hans Yssel,* Maria Fernanda Rios Grassi,[†,‡] and Vincent Vieillard*

Zika virus (ZIKV) is a mosquito-borne flavivirus that has emerged as a global concern because of its impact on human health. ZIKV infection during pregnancy can cause microcephaly and other severe brain defects in the developing fetus and there have been reports of the occurrence of Guillain-Barré syndrome in areas affected by ZIKV. NK cells are activated during acute viral infections and their activity contributes to a first line of defense because of their ability to rapidly recognize and kill virus-infected cells. To provide insight into NK cell function during ZIKV infection, we have profiled, using mass cytometry, the NK cell receptor-ligand repertoire in a cohort of acute ZIKV-infected female patients. Freshly isolated NK cells from these patients contained distinct, activated, and terminally differentiated, subsets expressing higher levels of CD57, NKG2C, and KIR3DL1 as compared with those from healthy donors. Moreover, KIR3DL1$^+$ NK cells from these patients produced high levels of IFN-γ and TNF-α, in the absence of direct cytotoxicity, in response to in vitro stimulation with autologous, ZIKV-infected, monocyte-derived dendritic cells. In ZIKV-infected patients, overproduction of IFN-γ correlated with STAT-5 activation ($r = 0.6643$; $p = 0.0085$) and was mediated following the recognition of MHC class 1–related chain A and chain B molecules expressed by ZIKV-infected monocyte-derived dendritic cells, in synergy with IL-12 production by the latter cells. Together, these findings suggest that NK cells contribute to the generation of an efficacious adaptive anti-ZIKV immune response that could potentially affect the outcome of the disease and/or the development of persistent symptoms. ***The Journal of Immunology*****, 2021, 207: 1333–1343.**

Zika virus (ZIKV) is a mosquito-borne flavivirus related to Dengue virus (DENV), yellow fever virus, and West Nile virus (1). During the first decades since its first discovery in the 1950s in Africa (2), ZIKV received little attention, remaining confined to the equatorial belt in Africa and Asia. The early clinical picture of natural human ZIKV infection was mainly associated with self-limiting symptoms, including fever, rash, and conjunctivitis. Recently however, ZIKV has emerged as a global concern because of its pandemic potential and its impact on human health with more than 500,000 infected individuals between 2015 and 2016 (3). In 2016, the World Health Organization has declared this virus a public health emergency of international concern because to its ability to cause Guillain-Barré syndrome in adults and birth defects, in particular microcephaly, in newborns from infected women (4–6).

ZIKV is primarily transmitted to humans by the bite of infected mosquitoes from the *Aedes aegypti* family (7). Viral entry into permissive dendritic cells (DC) facilitates the traffic of ZIKV to draining lymph nodes and other lymphoid tissues through DC-specific ICAM-3-grabbing nonintegrin (DC-SIGN), one of the main cellular receptors for this virus (8). In response, the infected host produces early type I IFNs, to mount a rapid and potent innate defense against ZIKV (9). This first innate immune response is responsible for the recruitment of monocytes to the inflammatory site, permitting the priming of NK cell activity during arbovirosis (10, 11).

NK cells are critical effectors of the innate immune response and represent a first line of defense against a variety of viral infections, including those caused by arboviruses (12–15). There is abundant proof for an early control of infectious disease by NK cells and further evidence for a direct role of these cells in protection against

*Sorbonne Université, UPMC, Inserm U1135, CNRS ERL 8255, Centre d'Immunologie et des Maladies Infectieuses, Paris, France; [†]FIOCRUZ, Salvador, Brazil; [‡]Escola Bahiana de Medicina e Saúde Pública, Salvador, Brazil; [§]UPMC Univ Paris 06, Plateforme de Cytométrie, UMS30–LUMIC, Faculté de Médecine Pierre et Marie Curie, Site Pitié-Salpêtrière, Paris, France; and [¶]Secretaria de Saúde da Bahia, Salvador, Bahia, Brazil

[1]C.M., G.A.N.Q, and A.C. contributed equally to this work.

[2]Current address: Université Côte d'Azur, CNRS UMR7275, Institut de Pharmacologie Moléculaire et Cellulaire (IPMC), Valbonne, France

ORCIDs: 0000-0003-1033-2992 (C.M.); 0000-0003-1272-6872 (A.C.); 0000-0002-7538-3558 (L.L.G.); 0000-0002-7440-5495 (A.M.-K.); 0000-0002-2610-9915 (A.S.); 0000-0003-2665-7417 (C.B.); 0000-0001-7454-1836 (H.Y.); and 0000-0002-9362-3922 (V.V.).

Received for publication October 19, 2020. Accepted for publication June 23, 2021.

This work was supported in part by the European Union Horizon 2020 ZIKAlliance Program (grant agreement 734548) and by the Coordination of Superior Level Staff Improvement-Brazil (CAPES Finance Code 001). C.M. received a Ph.D. fellowship from the French Ministry of Education; L.L.G. received a grant from the French Society for Cytometry; and M.F.R.G. is a research fellow of the National Council for Scientific and Technological Development (CNPq) and Foundation for the Development of Private Higher Education from Brazil.

C.M., H.Y., M.F.R.G., and V.V. designed the study; L.L.G., A.C.B., A.S., and M.F.R.G. were in charge of patient care, clinical data, and biological samples; C.M., G.A.N.Q., L.L.G., and N.T. performed experiments; A.C., A.M.-K., and C.B. designed and performed the mass cytometry analyses; V.V. wrote the first draft of the manuscript with critical input from H.Y. All authors approved the final version of the manuscript.

Address correspondence and reprint requests to Dr. Vincent Vieillard, Centre d'Immunologie et des Maladies Infectieuses (CIMI-Paris), Hôpital Pité-Salpêtrière, 91 Boulevard de l'Hôpital, 75013 Paris, France. E-mail address: vincent.vieillard@sorbonne-universite.fr

The online version of this article contains supplemental material.

Abbreviations used in this article: DC, dendritic cell; DC-SIGN, DC-specific ICAM-3–grabbing nonintegrin; DENV, Dengue virus; MIC, MHC class I–related chain; Mo-DC, monocyte-derived DC; RQ, relative quantification; SB, staining buffer; SPADE, spanning-tree progression analysis of density-normalized events; TP1, timepoint 1; TP2, timepoint 2; viSNE, visualization of *t*-distributed stochastic neighbor embedding; ZIKV, Zika virus.

viral infections comes from studies of patients with selective NK cell deficiencies, a condition that leads to the development of fulminant viral infections (16, 17). The importance of these cells is also underscored by the development of escape mechanisms by many viruses (i.e., HIV, herpes, and hepatitis viruses) to thwart NK cell responses (18). NK cell activity is shaped by the integration of signals that arise from the binding of a vast array of receptors present on the surface of these cells. They include not only inhibitory receptors, like KIR-L and NKG2A, but also activating receptors, such as the natural cytotoxicity receptors (NKp30, NKp44, and NKp46), NKG2D, and NKG2C. Although ligands for inhibitory receptors are mostly MHC class I molecules, those for activating receptors, exemplified by MHC class I–related chain (MIC)–A, MIC-B, and ULBP-1 to -6 for the NKG2D receptor, are diverse and their expression is upregulated under conditions of cellular stress, in particular during viral infection thereby allowing NK cells to specifically eliminate harmful infected host cells (19). When activating signals predominate, NK cells produce an array of proinflammatory cytokines, most importantly IFN-γ and TNF-α, in parallel with the initiation of their cytotoxic functions (20–22). Despite substantial progress in understanding ZIKV-specific immune responses in individuals, little is known about the role of NK cells in the pathogenesis of Zika fever. With respect to their activity in response to infection with other flaviviruses, we and others have observed that NK cells become activated and rapidly expand following infection of the host with DENV (10, 14, 23). Moreover, DENV type 2 was found to inhibit glycogen synthase kinase 3 activity and subsequently induce MIC-A expression in monocyte-derived DC (Mo-DCs), resulting in a specific increase in IFN-γ and TNF-α production in the absence of cytotoxicity, by autologous NK cells (15). It has previously been shown that ZIKV inhibits NK cell cytotoxicity by upregulating the expression of MHC class I molecules in response to IFN-β (24), whereas a protective role of NK cells against ZIKV infection was reported in mice (25).

In the present work, we have conducted a detailed phenotypic and functional analysis of NK cells by mass cytometry during acute infection of patients with ZIKV and have characterized in vitro the role of NK cell receptors and their ligands in the context of autologous ZIKV-infected Mo-DCs.

Materials and Methods

Patients, healthy controls, and sample preparation

Peripheral blood samples from 17 ZIKV-infected patients were obtained during the ZIKV outbreak that occurred in the Salvador area (Brazil) between March 2016 and December 2016. Samples from patients who had developed symptoms included fever, arthralgia, and asthenia and who visited the emergency room of a medical center in Salvador (Bahia, Brazil) were collected at the admission (timepoint 1 [TP1]) and 13–19 d later (timepoint 2 [TP2]). Molecular diagnosis of ZIKV infection was confirmed for each of the patients using PCR, as described (26). Ten healthy volunteers were used as negative controls. Patients and controls were PCR negative for chikungunya, yellow fever virus, and DENV infections. PBMCs were isolated from blood samples by standard density centrifugation, and then frozen at −150°C.

The study was conducted in accordance with the principles of the Declaration of Helsinki, as well as French statutory and regulatory law, and received approval from the Institutional Review Board of FIOCRUZ (protocol numbers 1.159.814 and 1.593.256/CAAE 55882016.6.0000.0040). Patients received information about research to be performed on their biological samples and provided written informed consent to participate.

Staining and mass cytometry acquisition

The 40 mAbs used for PBMC labeling were in-house conjugated to metal isotopes using MaxPAR Ab Conjugation Kits (Fluidigm), following the manufacturer's recommendations (Supplemental Table I) indicated by a star. Conjugated Abs were diluted to 100 times the working concentration in PBS Ab Stabilization Solution (Candor Bioscience) and stored at 4°C.

For each sample, PBMCs were thawed rapidly, incubated with a 50 μM solution of 127-IdU Cell-IDTM (Fluidigm) for 25 min at 37°C, followed by the addition of 2.5 μM 103Rh Cell-ID-Intercalator (Fluidigm) for 5 min at 37°C. Cells were then washed with staining buffer (SB; 1xPBS with 0.5% BSA and 0.02% sodium azide), and surface markers were stained following a multistep protocol. After Fc blocking, cells were incubated with a first Ab mix targeting chemokine receptors during 15 min, then with a second Ab mix targeting the other surface markers for 30 min at room temperature. After the 45 min of incubation, cells were washed with SB, fixed for 15 min with paraformaldehyde (Sigma-Aldrich) at a final concentration of 2%, permeabilized with methanol (Sigma-Aldrich) for 10 min and then intracellular stained for 60 min at +4°C. Cells were washed twice with SB and incubated overnight in 2% paraformaldehyde with 1:4000 the iridium intercalator [pentamethylcyclopentadienyl-Ir(III)-dipyridophenazine; Fluidigm] at 4°C, and frozen at −80°C, as described (27, Meghraoui-Kheddar, A. B.G. Chousterman, N. Guillou, S.M. Barone, S. Granjeaud, H. Vallet, A. Cornau, K. Guessous, A. Boissonnas, J.M. Irish, and C. Combadière, manuscript posted on bioRxiv, DOI: 10.1101/2020.05.29.123992).

Before acquisition, cells were thawed rapidly, resuspended in distilled-deionized water at 10^6 cells per mL and mixed with 4-Element EQ Beads (Fluidigm) and passed through a cell strainer cap with 35-mm pores (BD Biosciences). Cell events were acquired on the CyTOF Helios Mass Cytometer (Fluidigm) and CyTOF software version 6.7.1014 (Fluidigm) at the "Plateforme de Cytométrie de L'hôpital Pitié-Salpêtrière (CyPS)," Paris, France. Cytometry standard files produced on the CyTOF Helios were normalized using MatLab Compiler software normalizer based on the signals of the 4-Element EQ beads (Fluidigm) using MatLab Compiler software as recommended by the software developers.

Mass cytometry data analysis

After beads have been removed by an exclusion gate, intact single cells were gated on the basis of iridium intercalator DNA staining and live cells were selected on the basis of 103Rh before cell subsets analysis. The different analyzes were performed only with the samples with at least 2000 events.

To identify the main circulating immune populations, cell clustering was performed using Spanning-tree Progression Analysis of Density-normalized Events (SPADE) (28) in Cytobank platform (29), applying a down-sampling of 10% and targeting 50 nodes based on all the markers of the panel (Supplemental Table I). Identification of metaclusters, representing immune cell populations, were expert driven based on the median expression of all the markers in each node (Supplemental Table I).

Then, after the concatenation of samples from the same condition into a single group, a visualization of *t*-distributed stochastic neighbor embedding (viSNE) analysis was performed using the Cytobank platform based on the expression of the NK cells following markers: CD56, CD57, CD16, NKG2A, NKG2C, KIR2DL1, KIR2DL2L3, KIR3DL1, HLA-DR, IFN-γ, pSTAT-5, and Ki-67.

The viSNE (implementation of *t*-SNE) (30) was used to rearrange, by an unsupervised approach, cells in the different groups of the study in a common two-dimensional map, according to their expression profile of markers (Supplemental Table I).

A citrus analysis was performed using markers previously cited to identify the specific NK signature timepoint of the study.

To check discoveries from the unsupervised analysis, manual gating was done using a classical gating strategy to identify NK cells: $CD33^-CD14^-CD3^-CD56^+$ and the NK cells markers previously cited to be used in our unsupervised analyze. Then data were collected using GraphPad PRISM and a statistical analysis was done as discussed in the specific section of the materials and methods.

Cell isolation and generation of Mo-DCs

Monocytes were positively purified using $CD14^+$ beads (Miltenyi Biotec) from fresh PBMC isolated from buffy coat samples of healthy donors (Etablissement Français du Sang), and cultured for 6 d in the presence of 50 ng/ml IL-4 and 100 ng/ml GM-CSF (BioTechne). Successful differentiation of Mo-DCs was verified by the presence of CD1a (HI149), DC-SIGN (DCN46), CD40 (5C3) (all from BD Pharmingen), and HLA-DR (Immu-357; BioLegend) expression and the absence of CD14 (61D3; eBioscience) expression, as previously described (15).

Autologous NK cells were purified from the same healthy donors by negative selection using the NK Cell Isolation Kit (Miltenyi Biotec) (routinely purity > 98%) and subsequently cultured in RPMI supplemented with 10% human AB serum and 1,000 IU/ml of Proleukin-2 (Chiron) for 6 d. The purity was assessed using anti-CD45 (J.33; Coulter), anti-CD3 (UCHT1; eBioscience), and anti-CD56 (N901; Coulter) mAbs.

Preparation of ZIKV, infection of Mo-DCs, and coculture with autologous NK cells

The primary PF-25013-18 strain of ZIKV, kindly provided by Dr. Dorothée Missé (MIVEGEC, IRD Montpellier, France), was propagated in Vero cells (no. CCL-81; American Type Culture Collection) and harvested after 5 d of culture at 37°C. Cell debris was removed by centrifugation and aliquots were stored at −80°C, as previously described (31). Virus stock was titrated after extraction of cellular RNA from cell-supernatant using MirVanaTM miRNA Isolation Kit (Ambion). Quantitative PCR was next performed with the High Capacity cDNA Reverse Transcription Kit (Applied Biosystems) and MESA GREEN Quantitative PCR Master Mix (Eurogentec), using FLR ZIKV forward 5′-AGGACAGGCCTTGACTTTTC-3′ and reverse primer 5′-TGTTCCAGTGTGGAGTTC-3′. The level of gene expression was normalized to GAPDH. The copy of RNA (molecules per microliter) was determined using a dsDNA copy number calculator (http://cels.uri.edu/gsc/cndna.html), and estimated $\sim 5 \times 10^8$ copies per mL.

After 6 d of culture, 2×10^6 differentiated Mo-DCs were infected for 2 h at 37°C with 100 μl of virus stock (5×10^7 copies). Cells were washed twice to remove cell-free virus and cultured at a density of 10^6 cells per milliliter in 24-well plates RPMI supplemented with 10% FCS. As control, noninfected and Mo-DCs treated overnight with 10 μg/ml of LPS were used. Infected cells were fixed and permeabilized with Cytofix and Cytoperm (BD Pharmingen) during 30 min at 4°C, intracellularly stained with 5 μg/ml 3H5-1 antiflavivirus mAb (MilliporeSigma), specific to the envelope E glycoprotein of the flavivirus, then washed and stained with 1/500 of anti-mouse IgG1-FITC (Beckman Coulter). During this time, autologous NK cells were trashed or cultivated to be used in the functional assay. Staining was acquired on Gallios Cytometer (Beckman coulter) and analyzed using FlowJo software v09 (TreeStar).

Flow cytometry analyzes of Mo-DCs

Mo-DCs were first preincubated for 15 min at 4°C with an Fc blocking reagent (Miltenyi Biotec) to block nonspecific Fc receptor binding. Differentiation into Mo-DCs was assessed by flow cytometry with CD45-KO (J.33), HLA-DR-ECD (Immu-357) from Beckman Coulter, MIC-A–PE (159207; R&D Systems), MIC-B–PE (236511; R&D Systems), CD14-EF 780 (61D3; eBiosciences), and CD1a-allophycocyanin (HI149), CD83-PC7 (HB15e), and CD86-PB (GL1) from BioLegend. Isotype-matched Igs served as negative controls. The expression of ligands for NK cell receptors on Mo-DCs was assessed using specific mAbs: cells were first incubated with 1 μg/ml of fusion proteins (NKp30-Ig or NKp46-Ig, 1849-NK, and 1850-NK, respectively), anti–ULBP1-2-3 (170818, 165903, and 166510, respectively), or anti–MIC-A/-B (159207) mAbs from R&D Systems, for 2 h at 4°C. Cells were washed in PBS-BSA 0.5% and then stained using anti-human IgG1-PE at 1/50 dilution (Jackson ImmunoResearch) for Ig-fusion proteins, and anti-mouse hu-IgG2a-PE (Beckman Coulter) for anti–ULBP1-2-3 and anti–MIC-A/-B mAb or directly stained with allophycocyanin–anti–HLA-A,B,C (G46-2.6) mAbs for 1h at 4°C, as previously described (15, 32). Cells were acquired on a Gallios Ccytometer (Beckman Coulter). Flow cytometry data were analyzed using FlowJo software v. 9 (TreeStar).

NK cell degranulation and intracellular production of cytokines

For in vitro functional analysis, purified NK cells were incubated with autologous Mo-DCs at an E:T cell ratio from 1:1 in the presence of an anti-CD107a mAb (H4A3; Becton Dickinson) for 1 h, to measure degranulation. Cells were thereafter incubated for 4 h in the presence of Golgi Stop (4 μL per 6 mL of culture) and Golgi Plug (1 μL per mL of culture) from BD Biosciences and then were stained using anti–CD45-KO (J.33; Coulter), anti–CD3 (UCHT1; eBioscience) and anti-CD56 (N901; Coulter) mAbs. Cells were fixed, permeabilized using a Cytofix/Cytoperm Kit (BD Bioscience) during 30 mins at 4°C and then intracellularly stained for IFN-γ and TNF-α production, as described (23). In some experiments, Mo-DCs were preincubated with 10 μg/ml of 6D4 anti–MIC-A/-B (BioLegend) (2001; Groh), 10 μg/ml of W6/32 anti–HLA class I–blocking mAbs, 2.5 μM of Apilimod (formerly STA-5326), a specific inhibitor of IL-12 synthesis (33), or 10 μg/ml of LPS (both from Sigma-Aldrich).

Cells were acquired on a Gallios Cytometer (Beckman Coulter) and analyzed using FlowJo Software V09 (TreeStar).

For the ex vivo functional analysis, PBMC from seven randomly selected patients were rested during 2 h after thawing and then have been cultivated with K562 or not in the same condition as discussed for the in vitro functional analysis.

Real-time PCR analysis of IL-12 p35 and IL-12 p40

mRNA was extracted using the mirVana Kit (Thermo Fisher Scientific) and treated by DNAse (Ambion DNA-free; Invitrogen). Reverse transcription was then conducted with 200 ng mRNA using the Applied Biosystems High Capacity cDNA Reverse Transcription Kit (Thermo Fisher Scientific), according to the manufacturer's instructions. The real-time PCR was performed with the Applied Biosystems 7300 Real Time PCR system in the presence of SYBR-green. with 20 ng of cDNA and 10 μM of sense and reverse primers. After an initial step at 50°C for 2 min and 95°C for 10 min, a total of 40 cycles was performed. Each cycle consisted in 95°C for 15 s and 60°C for 1 min. At the end, a final cycle was performed at 95°C for 15 s, 60°C for 1 min, 95°C for 15 s, and 60°C for 15 s. The oligonucleotide sequences used for IL-12 p35, IL-12 p40, and RSP14, respectively: sense primers: CTCCTGGACCACCTCAGTTTG, CGGTCATCTGCCGCAAA, TGAAACCTTCCCTGGCCT-ACG; reverse primers: GGTGAAGGCATGGGAACATT, TGCCCATTCGCTCCAAGA, and GCTGCTGTGAGGGCTGGAGCTC. Data were analyzed with the double δ Ct (ΔΔCt) method using the 7300 Software System (Applied Biosystems) to determine relative quantification (RQ) of IL-12 p35 and IL-12 p40 gene expression: $RQ = 2^{(-\Delta\Delta Ct)}$ with ΔΔCt = ΔCt (sample) − ΔCt (calibrator); ΔCt (sample) = Ct (sample in test) − Ct (RSP14 in test); ΔCt = Ct (sample in calibrator) − Ct (RSP14 in calibrator), as previously described (15).

Statistical analysis

The nonparametric Mann–Whitney *U*, Kruskal–Wallis, and Wilcoxon tests were used as appropriate for the comparison of continuous variables between groups. Statistical analysis was performed using PRISM software (GraphPad).

Results

Proportion of immune cell subsets in ZIKV-infected patients analyzed by mass cytometry

We developed a mass cytometry 40 markers panel for a high-dimensional analysis of PBMCs subsets of ZIKV-infected patients and healthy controls. Surface markers were chosen to identify myeloid cells, T and B lymphocytes, and NK cells in addition to differentiation, activation, and functional markers (http://cels.uri.edu/gsc/cndna.html).

To establish the cellular heterogeneity of PBMCs, an SPADE clustering was performed using the same number of total live single cells of 17 ZIKV-infected patients, and eight healthy donors. The resulting 50 SPADE nodes were then grouped into five metaclusters corresponding to the canonical immune cell populations: $CD14^+$ myeloid cells, $CD3^-CD56^+$ NK cells, $CD4^+$ T cells, $CD8^+$ T cells, and $CD19^+$ B cells (Fig. 1A).

Analysis of metaclusters revealed that the frequencies of each cell population was conserved in PBMCs from ZIKV-infected patients at admission (TP1) and 13–19 d later (TP2), as compared with healthy donors (Fig. 1B), despite an interindividual degree of variability in ZIKV-infected patients (Fig. 1C). These data were confirmed with individual viSNE analyzes (data not shown), and suggest that distribution of the major immune cell subsets remains similar in donors and ZIKV-infected patients.

Major phenotypic features of NK cells from ZIKV-infected patients

Given the importance of NK cells in the early stage of infection, we performed a detailed analysis of the expression pattern of NK cells receptors in ZIKV-infected patients during the acute and postfebrile phase of infection. A viSNE dimensional reduction combined to SPADE revealed that several NK cell markers from $ZIKV^+$ patients are indistinguishable from those from healthy donors, irrespective of the timepoint tested (data not shown). Notably NK cells from $ZIKV^+$ and healthy donors expressed similar levels of CD16, NKG2A, KIR2DL1, KIR2DL2/DL3, CCR2, CXCR5, as well as exhaustion markers PD1, CTLA4, and Tim-3 (Fig. 2A and data not shown). However, NK cells from $ZIKV^+$ patients were found to express higher levels of CD57, NKG2C, and KIR3DL1, as compared with their healthy counterparts (Fig. 2A–C). Notably, overexpression of NKG2C was mainly associated with CD57 (Fig. 2B). These data were corroborated with a more systematic investigation using citrus algorithm, in which the three major specific metaclusters of TP1 and TP2 were $CD57^+NKG2C^+KIR3DL1^-$, $CD57^+NKG2C^-KIR3DL1^+$, and $CD57^+NKG2C^-KIR3DL1^-$ differentiated cell subsets (Supplemental Fig. 1).

To further characterize these responding NK cells during the acute phase of infection, markers of activation and cellular

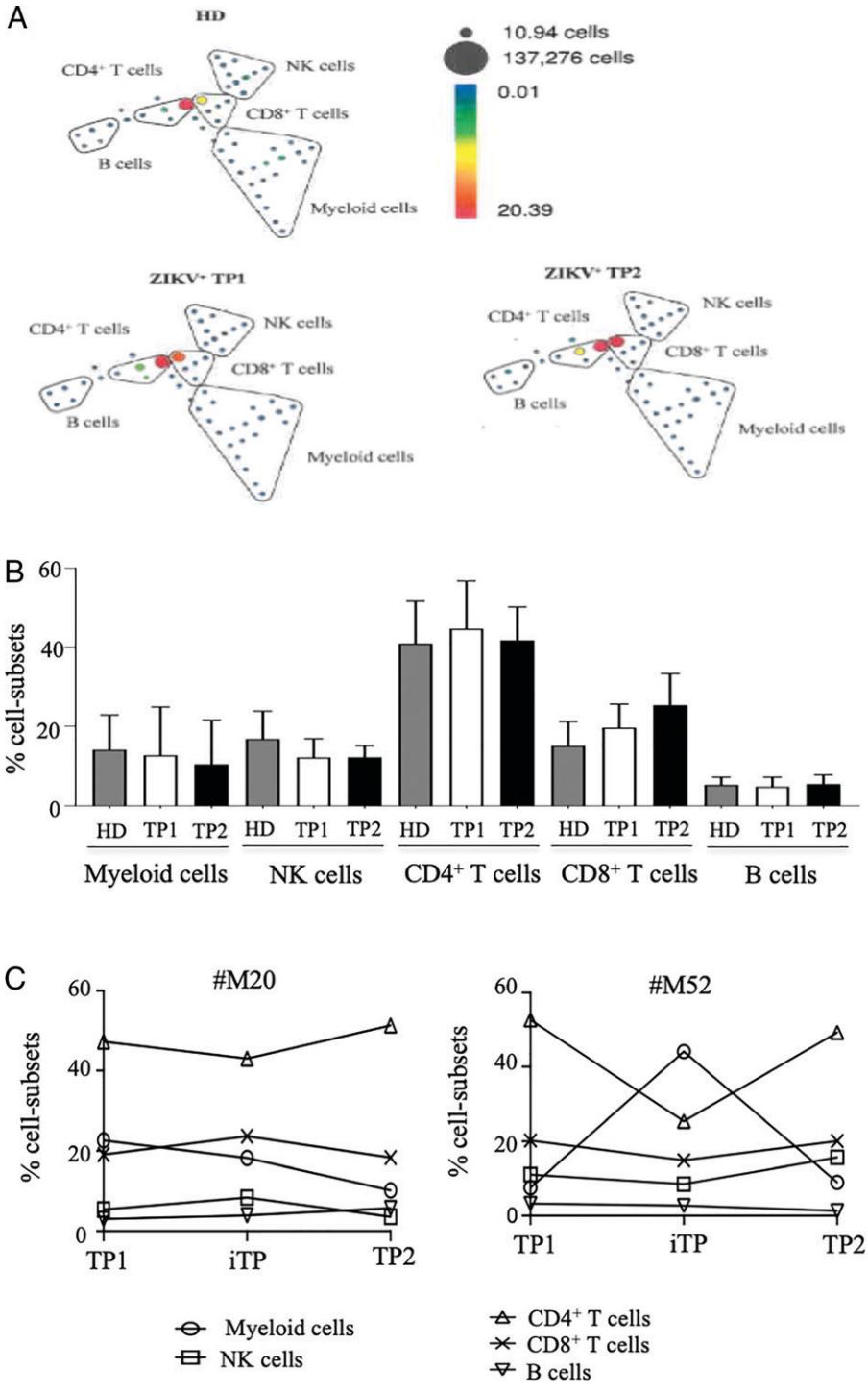

FIGURE 1. Impact of ZIKV on various cell-populations. (**A**) SPADE representations of cell-subsets distribution in the peripheral blood of ZIKV-infected patients. Cell-subsets are shown in mean of all healthy donors (HD) and ZIKV-infected patients ($ZIKV^+$) at the different timepoints (TP1 and TP2) after onset of the symptoms. For this general population SPADE, the channels used are as follows: CD19, CD4, CD16, CD11b, CD123, CD56, CD8, CD14, CD11c, CD33, HLA-DR, CD163, and CD3. (**B**) Distribution of cell-subsets in ZIKV-infected patients, compared with HDs. Data are done in frequency of $CD45^+$ cells from SPADE analysis. (**C**) Kinetic study of cell-subsets from two representative ZIKV-infected patients (no. M20 and no. M52).

proliferation were tested. A high percentage of NK cells from $ZIKV^+$ patients expressed the proliferation marker Ki-67 during TP1, compared with heathy donors, which subsequently declined throughout TP2 (Fig. 3A, 3B). A similar pattern was observed regarding HLA-DR–expressing cells, and cells coexpressing Ki-67 and HLA-DR (Fig. 3A, 3B). Importantly, HLA-DR was significantly overexpressed in both $NKG2C^+$ and $KIR3DL1^+$ NK cell subsets, whereas overexpression of Ki-67 was only observed in the $KIR3DL1^+$ NK cell subsets at TP1 (Fig. 3C). It seems, however, that expression of HLA-DR and Ki-67 decreases over time (Fig. 3C).

These data suggest that ZIKV infection is associated with the presence of activated and proliferating NK cell subsets expressing NKG2C or KIR3DL1.

ZIKV infection induces production of IFN-γ by NK cells

Given our finding that NK cells are activated and present specific phenotypic characteristics during acute ZIKV infection, we subsequently evaluated their functional capacities. Mass cytometry analysis revealed that the intracellular production of IFN-γ by NK cells was the most significant functional marker that distinguished ZIKV-infected patients from healthy donors ($p = 0.038$) (Fig. 4A, 4B). Although IFN-γ production was increased in $NKG2C^+$ NK cells from ZIKV-infected patients, the great majority of IFN-γ–producing cells expressed KIR3DL1. The latter population was increased in a statistically significant manner in $ZIKV^+$ patients ($p < 0.0001$), compared with healthy donors (Fig. 4C, 4D). Consequently, KIR3DL1 expression and IFN-γ production were also positively correlated in NK cells

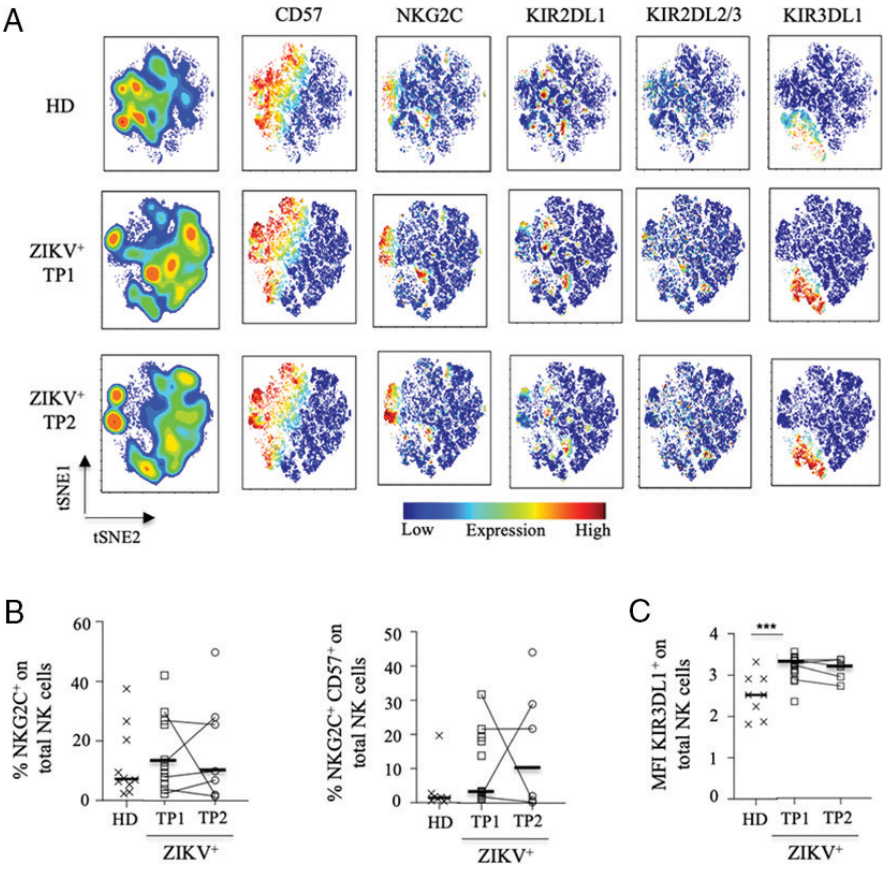

FIGURE 2. Expansion of adaptive NK cells from ZIKV-infected patients. (**A**) tSNE plots representing NK cells density in healthy donors (HD) and ZIKV-infected patients ($ZIKV^+$) PBMCs collected at the different timepoints (TP1 and TP2) after onset of symptoms in addition to NK cell receptors expression patterns in these groups. Plots represent merged files of each group of individuals. The settings used for the viSNE run were as follow: equal event sampling (12,468 events each), markers (CD16, CD56, CD57, NKG2A, NKG2C, KIR2DL1, KIR2DL2L3, KIR3DL1, IFN-γ, Ki-67, and pSTAT-5), iterations (7500), perplexity (30), and θ (0.7). (**B**) Frequency of $NKG2C^+$ and $CD57^+NKG2C^+$ NK cells (or NKG2C and CD57/NKG2C-expressing NK cells). (**C**) Mean of fluorescence intensity (MFI) of $KIR3DL1^+$ expression. Black lines represent the median of 10 HD, 15 TP1, and 7 TP2. An unpaired Mann–Whitney *U* test was performed between HD and TP1 groups and a paired Wilcoxon test was performed between TP1 and TP2 groups. ***$p < 0.0001$.

from $ZIKV^+$ patients at TP1 ($r = 0.8143$, $p = 0.0004$) (Fig. 4E). Interestingly, the frequency of IFN-γ production was significantly increased in KIR3DL1-expressing NK cells, as compared with $KIR3DL1^-$ cells in ZIKV-infected patients ($p < 0.0001$), whereas expression in NK cells from healthy donors remained close to baseline levels (Fig. 4F).

For validation, we next assessed the functional activity of NK cells by a standard flow cytometry assay in PBMC from ZIKV-infected patients. Fig. 5A shows that intracellular production of IFN-γ and TNF-α production by NK cells was significantly increased in $ZIKV^+$ patients, as compared with healthy controls. In contrast, the capacity of NK cells to release cytotoxic granules, as demonstrated by the expression of CD107a in the presence of K562 target cells, was not increased in ZIKV-infected patients, as compared with healthy donors (Fig. 5A).

To confirm these functional results, we also used an in vitro model of activated NK cells cocultured with autologous ZIKV-infected Mo-DCs. At 48 h postinfection by ZIKV, up to 48% of Mo-DCs were infected (Supplemental Fig. 2A). Except for the DC-SIGN receptor, the expression of most of the costimulatory molecules were upregulated in both bystander and infected Mo-DCs (data not shown). In line with data observed in ZIKV-infected patients (Fig. 5A), NK cell degranulation was not enhanced in NK cells cocultured with autologous ZIKV-infected Mo-DCs (Fig. 5B). In contrast, infected Mo-DCs induced enhanced production of IFN-γ and TNF-α in a statistically significant manner ($p = 0.016$ for both cytokines) by autologous NK cells, as compared with noninfected Mo-DCs (Fig. 5B). Importantly, the production of IFN-γ and TNF-α by autologous NK cells was strongly inhibited in experiments carried out with *trans*-well chambers (Supplemental Fig. 3A), suggesting that cell-cell contact is necessary for cytokine production by NK cells.

IL-12 p35 (14.3 ± 3.4-fold increased) and p40 (15.7 ± 1.5-fold increased) gene expression was significantly increased in Mo-DCs infected by ZIKV, as compared with noninfected cells, similarly to that observed after LPS treatment (Fig. 6A). Consistently, the intracellular production of IFN-γ and TNF-α by NK cells was strongly decreased after coculture with ZIKV-infected Mo-DCs pretreated with 2.5 μM of Apilimod (Fig. 6B). To gain inside in the signaling pathway, we determined phosphorylated STAT-5 (pSTAT-5) levels within NK cells from ZIKV-infected patients. As shown in Fig. 6C, pSTAT-5 levels were strongly increased in $ZIKV^+$ NK cells, as compared with those from healthy individuals, in a time-dependent manner (Fig. 6D), and statistically correlated with IFN-γ production by these cells ($r = 0.6643$, $p = 0.0085$) (Fig. 6E). Notably, pSTAT-5 was significantly increased in NK cells expressing NKG2C ($p = 0.050$) or KIR3DL1 ($p = 0.002$) (Supplemental Fig. 3B). To confirm the specific induction of pSTAT-5 by NK cells in the presence of ZIKV, we tested in vitro the expression of other activated STAT proteins (pSTAT-1, -3, and -6). Fig. 6F shows that only pSTAT-5 expression is increased after cocultured with autologous ZIKV-infected Mo-DC.

In conclusion, the production of cytokines induced by ZIKV is associated with the activation of the STAT-5 signaling pathway in NK cells and the production of IL-12 by the infected Mo-DCs.

Expression of ligands for NK cell receptors in ZIKV-infected Mo-DCs

We next sought to identify ligands for NK cell receptors on Mo-DCs that could contribute to the phenotypic and functional alterations of NK cells during acute ZIKV infection. Postinfection, a slight but distinct increase in the expression of MHC class I molecules, the ligands of KIR, was observed in Mo-DCs (Fig. 7A, 7B). Importantly, the frequency of MIC-A and MIC-B (MIC-A/B), two ligands of NKG2D, were significantly induced in ZIKV-infected Mo-DCs, as compared with LPS-treated and noninfected control

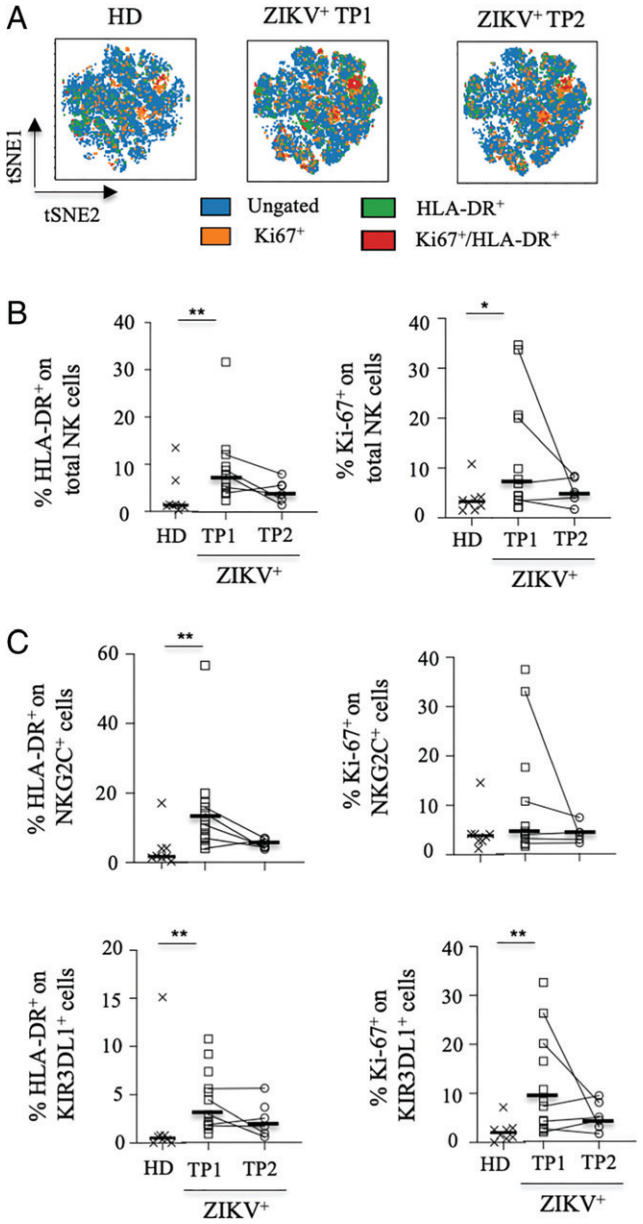

FIGURE 3. Cellular activation of NK cells from ZIKV-infected patients. (**A**) tSNE visualization of the cell activation (HLA-DR) and cell proliferation (Ki-67) markers in NK cells from healthy donors (HD) and ZIKV-infected patients (ZIKV$^+$) at the different timepoints (TP1and TP2) after onset of the symptoms. Plots represent merged files of each group of individuals. The parameters of viSNE are noted in the legend of Fig. 2B. (**B**) Frequency of HLA-DR and Ki-67 expression on total CD3$^-$CD56$^+$ NK cells. Black lines represent the median. (**C**) Frequency of HLA-DR– or Ki-67–expressing NKG2C$^+$ and KIR3DL1$^+$ NK cell subsets from HD (n = 8) and ZIKV-infected patients (ZIKV$^+$) at different timepoints (TP1, n = 13; TP2, n = 6) after onset of the symptoms. Black lines represent the median. An unpaired Mann–Whitney U test was performed between HD and TP1 groups, whereas a paired Wilcoxon test was performed between TP1 and TP2 groups. *$p < 0.01$, **$p < 0.001$.

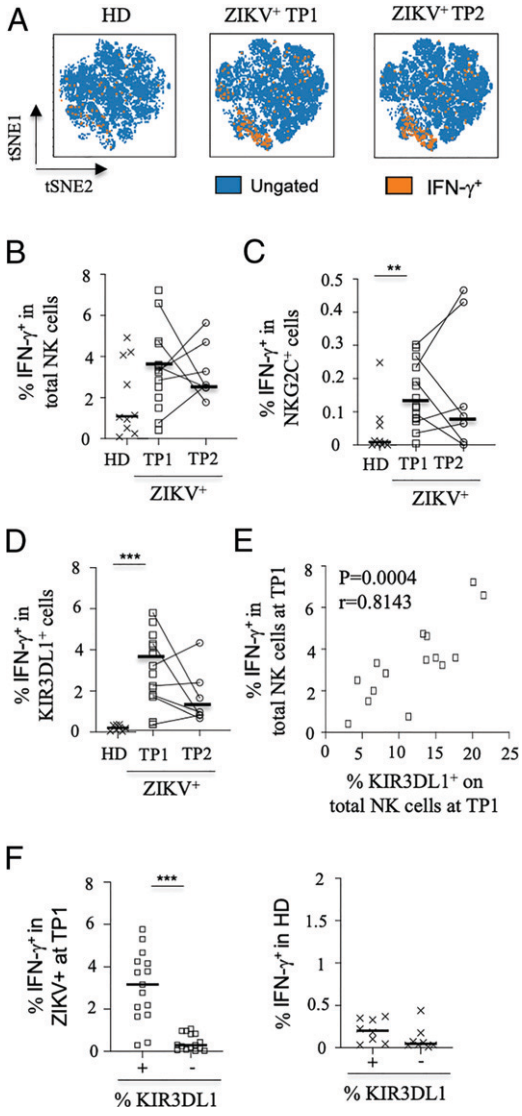

FIGURE 4. Intracellular production of IFN-γ in NK cells from ZIKV-infected patients. (**A**) tSNE visualization of IFN-γ–producing NK cells from healthy donors (HD) and ZIKV-infected patients at the different timepoints (TP1 and TP2) after onset of the symptoms. Plots represent merged files of each group of individuals. (**B**) Frequency of intracellular production of IFN-γ in total CD3$^-$CD56$^+$ NK cells. (**C**) Frequency of IFN-γ–positive CD3$^-$CD56$^+$ NK cells expressing NKG2C. (**D**) Frequency of IFN-γ–positive CD3$^-$CD56$^+$ NK cells expressing KIR3DL1. Data were obtained from HD (n = 8) and ZIKV-infected patients (ZIKV$^+$) at different timepoints (TP1, n = 15; TP2, n = 7) after onset of the symptoms. Black lines represent the median. An unpaired Mann–Whitney U test was performed between HD and TP1 groups, whereas a paired Wilcoxon test was performed between TP1 and TP2 groups. **$p < 0.001$, ***$p < 0.0001$. (**E**) Correlation between IFN-γ production of total CD3$^-$CD56$^+$ NK cells and frequency of KIR3DL1 expression by NK cells from ZIKV-infected patients at TP1. (**F**) Frequency of intracellular production of IFN-γ in CD3$^-$CD56$^+$ NK cells expressing or not KIR3DL1 in HD and ZIKV-infected patients (ZIKV$^+$) at TP1. Data are extrapolated from the Citrus analysis. Black lines represent the median. An unpaired Mann–Whitney U test was performed between KIR3DL1$^+$ and KIR3DL1$^-$ NK cells. ***$p < 0.0001$.

cells (Fig. 7A, 7B); upregulation of MIC-A expression is, however, more significant (p = 0.001) than that of MIC-B (p = 0.025) in ZIKV-infected Mo-DCs, as compared with noninfected control cells (Fig. 7B). In contrast, Mo-DCs infected by ZIKV were indistinguishable from those of noninfected controls subjects in terms of cell surface expression of other cellular ligands for major NK-activating receptors, including ULBP family proteins for NKG2D, and ligands of NKp30 and NKp46 (Supplemental Fig. 3C). Consistently, 73 to 93% of the ZIKV-infected cells expressed MIC-A/B (Supplemental Fig. 2B), and the level of NKG2D expression was downmodulated after a 5-h period of coculture with ZIKV-infected autologous Mo-DCs, as compared with noninfected target cells. In contrast, cell surface expression levels of NKp30 and NKp46, two

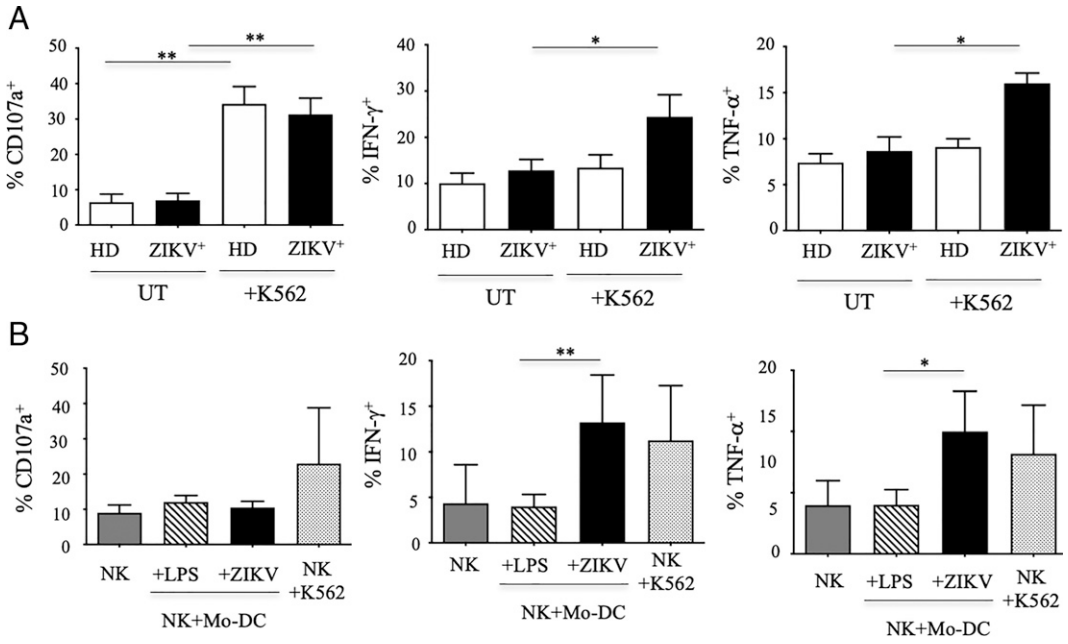

FIGURE 5. Functional activity of NK cells mediated by autologous ZIKV-infected Mo-DCs. (**A**) In vivo degranulation and production of IFN-γ and TNF-α by NK cells from healthy donors (HD; open bars) and ZIKV-infected patients (ZIKV$^+$; black bars) at TP1. Experiments are performed with untreated PBMC (UT) or in the presence of K562 target cells (+K562) at an E:T cell ratio of 1/1. Data are shown for five HDs and five ZIKV-infected patients. (**B**) In vitro degranulation and production of IFN-γ and TNF-α by purified untreated NK cells (gray bars), and NK cells cocultured with LPS-treated (+LPS; hatched bars) or ZIKV-infected (+ZIKV; black bars) autologous Mo-DCs. Experiments in the presence of K562 target cells (dotted bars) served as positive controls. Data are shown for seven different individuals. *$p = 0.05$, **$p = 0.001$.

other major activating NK receptors, remained unchanged following coculture with ZIKV-infected target cells (Supplemental Fig. 2C).

Together, these data strongly suggest that MIC-A/B plays a key role in the control of ZIKV infection by NK cells.

Engagement of MIC-A/B with NKG2D triggers cytokine production by NK cells

To gain insight into the mechanism(s) by which ZIKV induces cytokine production by NK cells in concert with MIC-A/B–expressing ZIKV-infected Mo-DCs, experiments were performed in the presence or absence of neutralizing anti–MIC-A/B mAbs. The production of IFN-γ and TNF-α was significantly decreased in the presence of neutralizing anti-NKG2D (Fig. 7C), and anti–MIC-A/B (Supplemental Fig. 3D) mAbs, at levels close to those observed with NK cells alone or cocultured with noninfected Mo-DCs. In contrast, in the presence of a neutralizing anti–MHC class I mAb, the production of IFN-γ and TNF-α remained unchanged (Supplemental Fig. 3D). Of note, the presence of neither anti–MIC-A/B nor anti–MHC class I mAbs modified the level of degranulation of autologous NK cells (data not shown).

To evaluate a possible additive/synergetic effect of IL-12 production and MIC-A/B expression by ZIKV-infected Mo-DCs on the intracellular cytokine production by autologous NK, we tested the combination of a treatment with the IL-12/IL-23 antagonist Apilimod and a neutralizing anti-NKG2D mAb. Stimulation of NK cells with ZIKV-infected target cells in the presence of both compounds resulted in a lower frequency of IFN-γ– and TNF-α–producing cells, as compared with cells treated with either Apilimod or anti-NKG2D mAb (Fig. 7C).

To further understand the relevance of these in vitro data, we finally assessed cytokine production by NK cells from ZIKV-infected patients in the presence or absence of neutralizing anti–MIC-A/B mAbs. Levels of both IFN-γ and TNF-α production were significantly decreased in NK cells from ZIKV-infected patients after treatment with anti–MIC-A/B mAbs, as compared with untreated cells, at similar levels as those observed in healthy donors (Fig. 7D).

Together, these data suggest that overexpression of MIC-A/B by Mo-DCs is a key element in the induction of cytokine production by NK cells, both in vitro and in patients infected by ZIKV.

Discussion

NK cells are known to rapidly respond during diverse acute viral infections in humans including those by arboviruses like chikungunya, yellow fever, and DENV (14, 23, 34, 35). However, the role of NK cells in the control of anti-ZIKV immunity needs to be better defined in view of the recent emergence and rapid spread of the Zika fever epidemic and the severe consequences of congenital ZIKV infection. Using high-dimensional mass cytometry, flow cytometry, and in vitro coculture assays in this study, we provide the first evidence, to our knowledge, that ZIKV infection may selectively shape the NK cell repertoire. Results revealed a massive activation of NK cells associated to the presence of adaptive CD57$^+$NKG2C$^+$ phenotype, as previously described in acute chikungunya virus and DENV infections (23, 34, 36). A limitation of this study is the absence of data concerning the seroprevalence of CMV with respect to the modulation of adaptive NK cells in ZIKV$^+$-infected patients; however, it was reported that 96.3% of the adolescents in the city of Belém in Brazil presented IgG Abs to CMV (37), suggesting that data on adaptive NK cells can be analyzed independently of the CMV serostatus.

In contrast to the overall NK cell repertoire, which contains a random distribution of KIRs in healthy donors, skewing of KIR repertoire toward self-specific KIRs has previously been observed in patients infected by some viruses (38). In this study, we show that NK cells from ZIKV$^+$ patients are preferentially associated with KIR3DL1, whereas an expansion of KIR2DL1$^+$-adaptive NK cells for DENV has been reported (23). The mechanism underlying the expansion of educated NK cells bearing self-specific KIRs remains

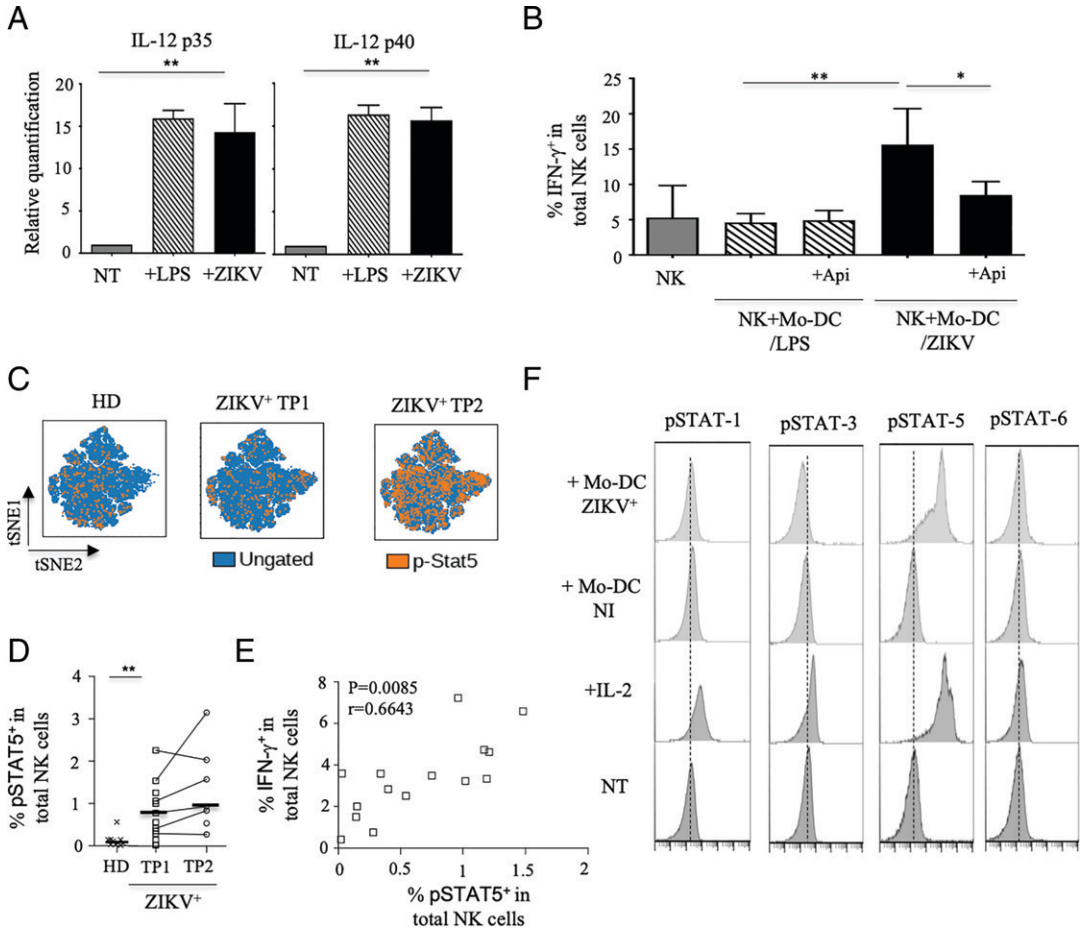

FIGURE 6. Cytokine production by NK cells from ZIKV$^+$ patients is associated to STAT-5 activation. (**A**) Quantification of IL-12 p35 and IL-12 p40 by real-time PCR in Mo-DCs infected by ZIKV. The bar graph shows the enrichment (*n*-fold) of RQ of IL-12 p35 (left panel) and IL-12 p40 (right panel) gene expression in noninfected (NT; gray bars), LPS-treated (+LPS; hatched bars) or ZIKV-infected (+ZIKV; black bars) Mo-DCs from three different individuals. (**B**) Intracellular production of IFN-γ and TNF-α by NK cells after pretreatment of target cells with 2.5 μM of Apilimod (+Api). Experiments are performed with purified NK cells (UT, gray bars) or NK cells cocultured with LPS-treated (NK + Mo-DC/LPS; hatched bars) or ZIKV-infected autologous Mo-DCs for 48 h (NK + DC/ZIKV, black bars). Data are shown in mean ± SD of seven experiments. $*p = 0.05$, $**p = 0.001$. (**C**) tSNE visualization of latent transcription factor STAT-5 activated by tyrosine phosphorylation (pSTAT5) in NK cells from healthy donors (HD) and ZIKV-infected patients (ZIKV$^+$) at different timepoints (TP1 and TP2) after onset of the symptoms. Plots represent merged files of each group of individuals. The settings used for the viSNE run were as follow: equal event sampling (44,400 events each), channels (CD16, CD56, CD57, NKG2A, NKG2C, KIR2DL1, KIR2DL2L3, KIR3DL1, CD38, HLA-DR, PD1, Tim3, CTLA4, IFN-γ, and Ki-67), iterations (7500), perplexity (30), and θ (0.7). (**D**) Frequency of pSTAT-5 expression in CD3$^-$CD56$^+$ NK cells from HD ($n = 10$) and ZIKV-infected patients (ZIKV$^+$) at different timepoints (TP1, $n = 15$; TP2, $n = 7$) after onset of the symptoms. Black lines represent the median. An unpaired Mann–Whitney *U* test was performed between HD and TP1 groups, whereas a paired Wilcoxon test was performed between TP1 and TP2 groups. (**E**) Correlation of intracellular production of IFN-γ and pSTAT-5 expression in total NK cells from ZIKV-infected patients at TP1. Data are extrapolated from the Citrus analysis. (**F**) In vitro expression of activated STAT (pSTAT-1, -3, -5, and -6) in NK cells cocultured with autologous Mo-DCs infected by ZIKV from an HD. Data were obtained using the "BD Phosflow Monocyte/NK cell Activation Kit" (catalog no. 562089). Untreated (NT) and IL-2–activated cells were used as controls. Dotted lines represent the median value observed in untreated NK cells.

elusive; although it can be hypothesized that HLA-presented viral peptides could modulate KIR/HLA interactions, as previously observed in several other viral infections (39–42). Together, the findings suggest an impact of education of NK cells during the acute phase of ZIKV infection. However, a genetic analysis of the KIR/HLA, combined with phenotypic and functional features of NK cells ZIKV-infected individuals. Another limitation was the low number the samples at the second timepoint (TP2), which reduces the statistical significance of the analysis. Thus, further prospective studies on a larger number of patients are necessary to draw firmer conclusions. Furthermore, it seems that activated and proliferating NK cells decrease over time after ZIKV infection, suggesting that intense NK cell activation and trafficking to and from tissues occurs early in ZIKV, and is associated with subsequent disease progression, providing an insight into the mechanism of clinical deterioration. Thus; it would be interesting to measure the proportion of circulating and resident CD69$^+$CD103$^+$CD49d$^+$ NK cells in different hematopoietic and nonhematopoietic tissues.

Given their functional capacities, it is important to determine whether NK cells play a role in the immune response to ZIKV infection. As previously reported for DENV infections (23, 24), ZIKV appears to impair the ability of NK cells to degranulate in infected patients. This impairment may be linked to high levels of MHC class I expression, as previously shown for other flavivirus infections (13, 24), whereas many other viruses downregulate levels of some MHC class I molecules (43). However, in contrast to DENV, infection by ZIKV does not induce the expression of the HLA-E molecule (44), suggesting that the functional capacity of NK cells is not directly mediated by NKG2C in ZIKV infection, as compared with DENV (14, 23). Consistently, we show that in ZIKV$^+$ patients, the frequency of IFN-γ$^+$ KIR3DL1$^+$ NK cells was significantly higher than that of IFN-γ$^+$NKG2C–expressing NK cells.

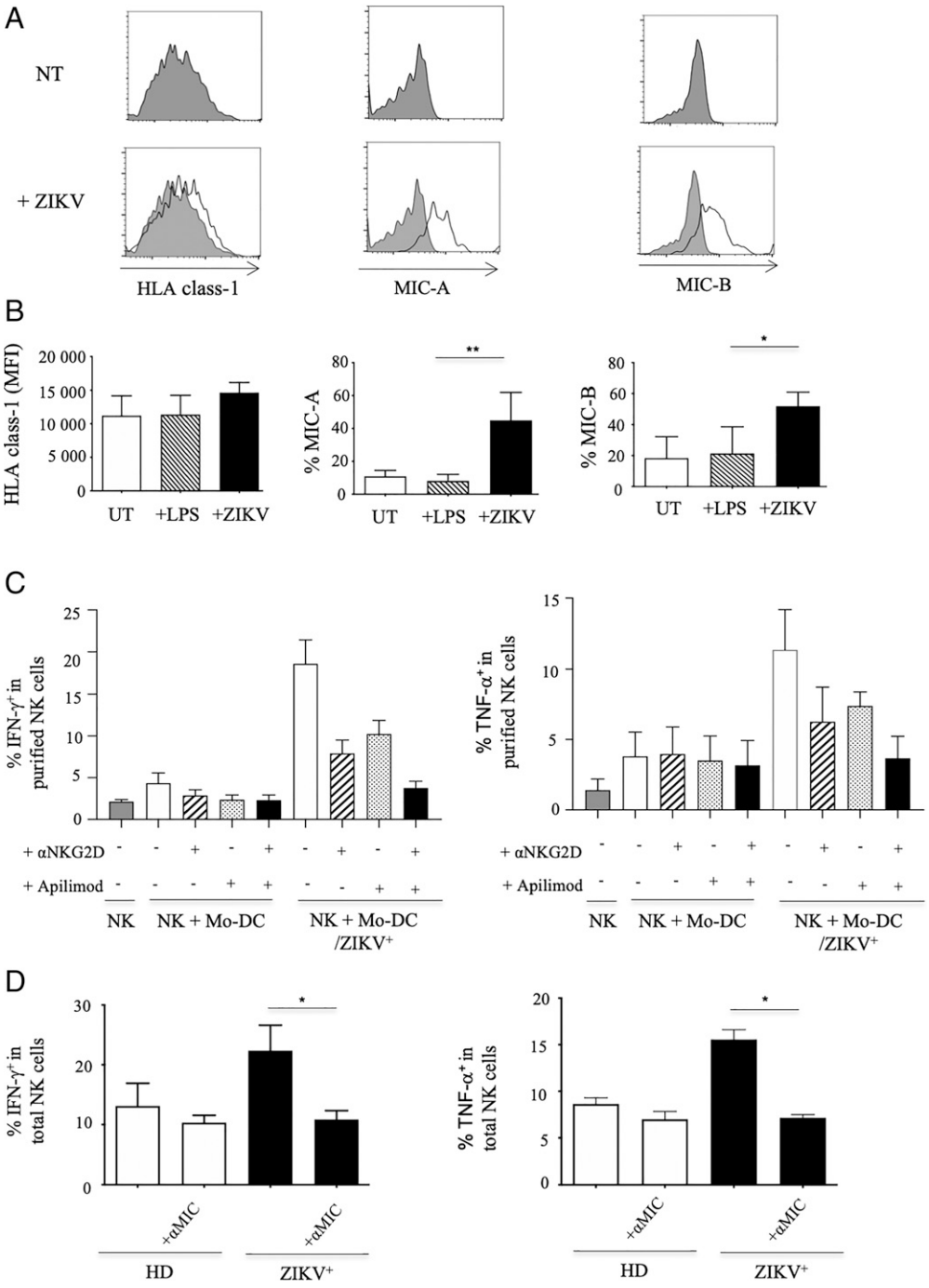

FIGURE 7. Expression of cellular ligands for NK receptors by Mo-DCs infected by ZIKV (**A**) Representative histograms of expression on noninfected (NT), and Mo-DCs infected by ZIKV for 48 h. Positive staining is represented by the open gray line. (**B**) Mean of fluorescence intensity (MFI) of MHC class I molecules expression and frequency MIC-A and MIC-B on untreated (NT, open bars), LPS-treated (+LPS; hatched bars) and ZIKV-infected (+ZIKV; black bars) Mo-DCs. Results are expressed as mean ± SD for five experiments. (**C**) Intracellular production of IFN-γ and TNF-α by NK cells after pretreatment of target cells with 10 μg/ml blocking 1D11 anti-NKG2D (+αNKG2D) mAbs and/or treated with 2.5 μM of Apilimod (+Apilimod). Experiments were performed with purified untreated NK cells (NK, gray bars), or in the presence of autologous Mo-DCs noninfected (Mo-DC) or infected by ZIKV for 48 h (NK + DC/ZIKV$^+$). Results are expressed as mean ± SD for three experiments. (**D**) Effect of pretreatment with 10 μg/ml 6D4 anti–MIC-A/B (+α-MIC) mAbs on the intracellular production of IFN-γ and TNF-α by NK cells from healthy donors (HD) and ZIKV-infected patients (ZIKV$^+$). Results are expressed as mean ± SD for seven experiments. *p = 0.05, **p = 0.001.

Production of cytokines by NK cells, measured by mass cytometry and confirmed after coculture with autologous ZIKV-infected Mo-DCs, is a key element in the control of ZIKV by NK cells. These data are further supported by previous results reporting that ZIKV-infected patients produce high levels of several immune mediators associated with NK cell function, such as IL-18, IFN-γ, and TNF-α (45). The production of IFN-γ and TNF-α by NK cells is also profoundly decreased after treatment of ZIKV-infected Mo-DCs with Apilimod, which selectively and potently inhibits the production of IL-12 (46), whereas IL-12 p35 and p40 transcripts are expressed to a higher extent in ZIKV-infected Mo-DCs. Surprisingly, results obtained from in vitro experiments, as well as from the mass cytometry analysis, also showed a massive phosphorylation of STAT-5 in NK cells from ZIKV-infected patients, confirmed in vitro by coculture with ZIKV-infected Mo-DCs, which strongly correlated with the frequency of IFN-γ$^+$ NK cells. Results obtained from the mass cytometry analysis showed that the phosphorylation of STAT-5 in NK cells from ZIKV-infected patients, confirmed in vitro by coculture with ZIKV-infected Mo-DCs, strongly correlated with the frequency of IFN-γ$^+$ NK cells. It has previously been shown that STAT-5 can upregulate the promoter activity of the IFN-γ–encoding *IFNG* genes (47). Furthermore, IL-2 or IL-12 phosphorylates STAT-5 to drive IFN-γ production in activated cells, which is even enhanced in the presence of IFN-γ (48, 49). These findings suggest that the activation of STAT-5 may be a mechanism through which activated NK cells could increase IFN-γ secretion in the presence of IL-12. Thus, it might be interesting to more precisely determine the signaling pathway(s) that are engaged in the phosphorylation of STAT-5 leading to the production of IFN-γ in ZIKV infection.

The importance of a cell-to-cell cross-talk for cytokine production by NK cells during ZIKV infection also prompted us to analyze, in

detail, the mechanism by which NK cells control infection. In vitro we observed that MIC-A and MIC-B expression was induced on ZIKV-infected Mo-DCs, whereas other ligands of NKG2D (ULBP-1 to 6), and those for NKp30 and NKp46 remained unchanged, as compared with uninfected cells, reminiscent to what has been observed for DENV (15). These data contrast with the, previously reported, small increase in the expression of activating NK cell ligands following ZIKV infection (24), and should be validated in DC from ZIKV-infected patients. The potential explanation for the discrepancies between the latter study and ours might be the difference in target cells; unlike using the A549 tumor lung carcinoma cell line, which expresses basal levels of stress molecules (50, 51), we used primary Mo-DCs from healthy donors in our experiments. MIC-A and MIC-B expression is generally not observed at the surface of normal cells but constitutively expressed in stress situations, like cancer and viral/bacterial infections (52). Furthermore, we observed that NKG2D expression was specifically downregulated in NK cells following coculture with ZIKV-infected target cells. These data are consistent with those of a previous report showing a degradation of the NKG2D receptor from the cell surface following its interaction with MIC-A/B (53). Our data suggest that an additive/synergistic effect of MIC-A/B and IL-12, produced by ZIKV-infected Mo-DCs, can trigger NK cells to produce high levels of proinflammatory cytokines, but fail to induce cytotoxicity.

Collectively, our data reveal an expansion of specific NK cells able to sense ZIKV via the NKG2D/MIC-A/B signaling pathway to induce STAT-5 and the production of proinflammatory cytokines. This specific mechanism could contribute to the generation of an efficacious adaptive anti-ZIKV immune response that may potentially affect both the outcome of the disease and/or the development of persistent symptoms.

Acknowledgments

We thank the Dr. Dorothée Missé (MIVEGEC, IRD Montpellier, France) for the ZIKV strain. We also thank Prof. Brigitte Autran and Dr. Christophe Combadière (CIMI-Paris, Paris, France) for helpful discussions. We are grateful to all patients and healthy volunteers for their participation in the study.

Disclosures

The authors declare no financial or commercial conflict of interest.

References

1. Wikan, N., and D. R. Smith. 2016. Zika virus: history of a newly emerging arbovirus. *Lancet Infect. Dis.* 16: e119–e126.
2. Dick, G. W., S. F. Kitchen, and A. J. Haddow. 1952. Zika virus. I. Isolations and serological specificity. *Trans. R. Soc. Trop. Med. Hyg.* 46: 509–520.
3. Baud, D., D. J. Gubler, B. Schaub, M. C. Lanteri, and D. Musso. 2017. An update on Zika virus infection. *Lancet* 390: 2099–2109.
4. Cao-Lormeau, V. M., A. Blake, S. Mons, S. Lastère, C. Roche, J. Vanhomwegen, T. Dub, L. Baudouin, A. Teissier, P. Larre, et al. 2016. Guillain-Barré Syndrome outbreak associated with Zika virus infection in French Polynesia: a case-control study. *Lancet* 387: 1531–1539.
5. Dos Santos, T., A. Rodriguez, M. Almiron, A. Sanhueza, P. Ramon, W.K. de Oliveira, G.E. Coelho, R. Badaró, J. Cortez, M. Ospina, et al. 2016. Zika virus and the Guillain-Barré Syndrome—Case series from seven countries. *N. Engl. J. Med.* 375: 1598–1601.
6. Rubin, E. J., M. F. Greene, and L. R. Baden. 2016. Zika Virus and Microcephaly. *N. Engl. J. Med.* 374: 984–985.
7. Kindhauser, M. K., T. Allen, V. Frank, R.S. Santhana, and C. Dye. 2016. Zika: the origin and spread of a mosquito-borne virus. *Bull. World Health Organ.* 94: 675–686C.
8. Carbaugh, D. L., R. S. Baric, and H. M. Lazear. 2019. Envelope Protein Glycosylation Mediates Zika Virus Pathogenesis. *J. Virol.* 93: e00113–e00119.
9. Yockey, L.J., K.A. Jurado, N. Arora, A. Millet, T. Rakib, K.M. Milano, A.K. Hastings, E. Fikrig, Y. Kong, T.L. Horvath, et al. 2018. Type I interferons instigate fetal demise after Zika virus infection. *Sci. Immunol.* 3: eaao1680.
10. Lum, F. M., D. Lee, T. K. Chua, J. J. L. Tan, C. Y. P. Lee, X. Liu, Y. Fang, B. Lee, W. X. Yee, N. Y. Rickett, et al. 2018. Zika Virus Infection Preferentially Counterbalances Human Peripheral Monocyte and/or NK Cell Activity. *MSphere* 3: e00120-e18.
11. Maucourant, C., G. A. N. Queiroz, A. Samri, M. F. R. Grassi, H. Yssel, and V. Vieillard. 2019. Zika virus in the eye of the cytokine storm. *Eur. Cytokine Netw.* 30: 74–81.
12. van Erp, E. A., M. R. van Kampen, P. B. van Kasteren, and J. de Wit. 2019. Viral Infection of Human Natural Killer Cells. *Viruses* 11: 243.
13. Maucourant, C., C. Petitdemange, H. Yssel, and V. Vieillard. 2019. Control of Acute Arboviral Infection by Natural Killer Cells. *Viruses* 11: 131.
14. Zimmer, C. L., M. Cornillet, C. Solà-Riera, K. W. Cheung, M. A. Ivarsson, M. Q. Lim, N. Marquardt, Y. S. Leo, D. C. Lye, J. Klingström, et al. 2019. NK cells are activated and primed for skin-homing during acute dengue virus infection in humans. *Nat. Commun.* 10: 3897.
15. Petitdemange, C., C. Maucourant, N. Tarantino, J. Rey, and V. Vieillard. 2020. Glycogen synthetase kinase 3 inhibition drives MIC-A/B to promote cytokine production by human natural killer cells in Dengue virus type 2 infection. *Eur. J. Immunol.* 50: 342–352.
16. Biron, C. A., K. S. Byron, and J. L. Sullivan. 1989. Severe herpesvirus infections in an adolescent without natural killer cells. *N. Engl. J. Med.* 320: 1731–1735.
17. Orange, J. S. 2006. Human natural killer cell deficiencies. *Curr. Opin. Allergy Clin. Immunol.* 6: 399–409.
18. Lodoen, M. B., and L. L. Lanier. 2005. Viral modulation of NK cell immunity. *Nat. Rev. Microbiol.* 3: 59–69.
19. Koehl, U., A. Toubert, and G. Pittari. 2018. Editorial: Tailoring NK Cell Receptor-Ligand Interactions: An Art in Evolution. *Front. Immunol.* 9: 351.
20. Gasser, S., and D. H. Raulet. 2006. Activation and self-tolerance of natural killer cells. *Immunol. Rev.* 214: 130–142.
21. Sun, J. C., and L. L. Lanier. 2011. NK cell development, homeostasis and function: parallels with $CD8^+$ T cells. *Nat. Rev. Immunol.* 11: 645–657.
22. Vivier, E., D. H. Raulet, A. Moretta, M. A. Caligiuri, L. Zitvogel, L. L. Lanier, W. M. Yokoyama, and S. Ugolini. 2011. Innate or adaptive immunity? The example of natural killer cells. *Science* 331: 44–49.
23. Petitdemange, C., N. Wauquier, H. Devilliers, H. Yssel, I. Mombo, M. Caron, D. Nkoghé, P. Debré, E. Leroy, and V. Vieillard. 2016. Longitudinal Analysis of Natural Killer Cells in Dengue Virus-Infected Patients in Comparison to Chikungunya and Chikungunya/Dengue Virus-Infected Patients. *PLoS Negl. Trop. Dis.* 10: e0004499.
24. Glasner, A., E. Oiknine-Djian, Y. Weisblum, M. Diab, A. Panet, D. G. Wolf, and O. Mandelboim. 2017. Zika Virus Escapes NK Cell Detection by Upregulating Major Histocompatibility Complex Class I Molecules. *J. Virol.* 91: e00785-17.
25. Duan, X., S. Li, G. Wong, D. Wang, H. Wang, J. Lu, Y. Bi, X. Lu, Y. Shi, J. Yan, et al. 2017. Natural killer cells are activated and play a protective role against ZIKA virus infection in mice. *Sci. Bull. (Beijing)* 62: 982–984.
26. Balm, M. N., C. K. Lee, H. K. Lee, L. Chiu, E. S. Koay, and J. W. Tang. 2012. A diagnostic polymerase chain reaction assay for Zika virus. *J. Med. Virol.* 84: 1501–1505.
27. Corneau, A., A. Cosma, S. Even, C. Katlama, R. Le Grand, V. Frachet, C. Blanc, and B. Autran. 2017. Comprehensive Mass Cytometry Analysis of Cell Cycle, Activation, and Coinhibitory Receptors Expression in CD4 T Cells from Healthy and HIV-Infected Individuals. *Cytometry B Clin. Cytom.* 92: 21–32.
28. Qiu, P., E. F. Simonds, S. C. Bendall, K. D. Gibbs, Jr., R. V. Bruggner, M. D. Linderman, K. Sachs, G. P. Nolan, and S. K. Plevritis. 2011. Extracting a cellular hierarchy from high-dimensional cytometry data with SPADE. *Nat. Biotechnol.* 29: 886–891.
29. Kotecha, N., P.O. Krutzik, and J.M. Irish, 2010. Web-based Analysis and Publication of Flow Cytometry Experiments. *Curr. Protoc. Cytom.* Chapter 10: Unit10.17. PMID: 20578106.
30. Amir, el-A.D., K.L. Davis, M.D. Tadmor, E.F. Simonds, J.H. Levine, S.C. Bendall, D.K. Shenfeld, S. Krishnaswamy, G.P. Nolan, and D. Pe'er, 2013. viSNE enables visualization of high dimensional single-cell data and reveals phenotypic heterogeneity of leukemia. *Nat. Biotechnol.* 31: 545–552.
31. Hamel, R., O. Dejarnac, S. Wichit, P. Ekchariyawat, A. Neyret, N. Luplertlop, M. Perera-Lecoin, P. Surasombatpattana, L. Talignani, F. Thomas, et al. 2015. Biology of Zika Virus Infection in Human Skin Cells. *J. Virol.* 89: 8880–8896.
32. Baychelier, F., A. Sennepin, M. Ermonval, K. Dorgham, P. Debré, and V. Vieillard. 2013. Identification of a cellular ligand for the natural cytotoxicity receptor NKp44. *Blood* 122: 2935–2942.
33. Cai, X., Y. Xu, A. K. Cheung, R. C. Tomlinson, A. Alcázar-Román, L. Murphy, A. Billich, B. Zhang, Y. Feng, M. Klumpp, et al. 2013. PIKfyve, a class III PI kinase, is the target of the small molecular IL-12/IL-23 inhibitor apilimod and a player in Toll-like receptor signaling. *Chem. Biol.* 20: 912–921.
34. Petitdemange, C., P. Becquart, N. Wauquier, V. Béziat, P. Debré, E. M. Leroy, and V. Vieillard. 2011. Unconventional repertoire profile is imprinted during acute chikungunya infection for natural killer cells polarization toward cytotoxicity. *PLoS Pathog.* 7: e1002268.
35. Marquardt, N., M. A. Ivarsson, K. Blom, V. D. Gonzalez, M. Braun, K. Falconer, R. Gustafsson, A. Fogdell-Hahn, J. K. Sandberg, and J. Michaëlsson. 2015. The Human NK Cell Response to Yellow Fever Virus 17D Is Primarily Governed by NK Cell Differentiation Independently of NK Cell Education. *J. Immunol.* 195: 3262–3272.
36. Paust, S., C. A. Blish, and R. K. Reeves. 2017. Redefining Memory: Building the Case for Adaptive NK Cells. *J. Virol.* 91: e00169-e17.
37. Guerra, A. B., L. Q. Siravenha, R. V. Laurentino, R. N. M. Feitosa, V. N. Azevedo, A. C. R. Vallinoto, R. Ishak, and L. F. A. Machado. 2018. Seroprevalence of HIV, HTLV, CMV, HBV and rubella virus infections in pregnant adolescents who received care in the city of Belém, Pará, Northern Brazil. *BMC Pregnancy Childbirth* 18: 169.

38. Kulkarni, S., M. P. Martin, and M. Carrington. 2008. The Yin and Yang of HLA and KIR in human disease. *Semin. Immunol.* 20: 343–352.
39. Alter, G., D. Heckerman, A. Schneidewind, L. Fadda, C. M. Kadie, J. M. Carlson, C. Oniangue-Ndza, M. Martin, B. Li, S. I. Khakoo, et al. 2011. HIV-1 adaptation to NK-cell-mediated immune pressure. *Nature* 476: 96–100.
40. Jost, S., and M. Altfeld. 2013. Control of human viral infections by natural killer cells. *Annu. Rev. Immunol.* 31: 163–194.
41. Townsley, E., G. O'Connor, C. Cosgrove, M. Woda, M. Co, S. J. Thomas, S. Kalayanarooj, I. K. Yoon, A. Nisalak, A. Srikiatkhachorn, et al. 2015. Interaction of a dengue virus NS1-derived peptide with the inhibitory receptor KIR3DL1 on natural killer cells. *Clin. Exp. Immunol.* 183: 419–430.
42. Wauquier, N., C. Petitdemange, N. Tarantino, C. Maucourant, M. Coomber, V. Lungay, J. Bangura, P. Debré, and V. Vieillard. 2019. HLA-C-restricted viral epitopes are associated with an escape mechanism from KIR2DL2^{+} NK cells in Lassa virus infection. *EBioMedicine* 40: 605–613.
43. Lobigs, M., A. Müllbacher, and M. Regner. 2003. MHC class I up-regulation by flaviviruses: Immune interaction with unknown advantage to host or pathogen. *Immunol. Cell Biol.* 81: 217–223.
44. Drews, E., A. Adam, P. Htoo, E. Townsley, and A. Mathew. 2018. Upregulation of HLA-E by dengue and not Zika viruses. *Clin. Transl. Immunology* 7: e1039.
45. Kam, Y. W., J. A. Leite, F. M. Lum, J. J. L. Tan, B. Lee, C. C. Judice, D. A. T. Teixeira, R. Andreata-Santos, M. A. Vinolo, R. Angerami, et al. Zika-Unicamp Network. 2017. Specific Biomarkers Associated With Neurological Complications and Congenital Central Nervous System Abnormalities From Zika Virus-Infected Patients in Brazil. *J. Infect. Dis.* 216: 172–181.
46. Wada, Y., R. Lu, D. Zhou, J. Chu, T. Przewloka, S. Zhang, L. Li, Y. Wu, J. Qin, V. Balasubramanyam, et al. 2006. Selective abrogation of Th1 response by STA-5326, a potent IL-12/IL-23 inhibitor. *Blood* 109: 1156–1164.
47. Gonsky, R., R. L. Deem, J. Bream, H. A. Young, and S. R. Targan. 2004. Enhancer role of STAT5 in CD2 activation of IFN-gamma gene expression. *J. Immunol.* 173: 6241–6247.
48. Gollob, J. A., E. A. Murphy, S. Mahajan, C. P. Schnipper, J. Ritz, and D. A. Frank. 1998. Altered interleukin-12 responsiveness in Th1 and Th2 cells is associated with the differential activation of STAT5 and STAT1. *Blood* 91: 1341–1354.
49. Herr, F., R. Lemoine, F. Gouilleux, D. Meley, I. Kazma, A. Heraud, F. Velge-Roussel, C. Baron, and Y. Lebranchu. 2014. IL-2 phosphorylates STAT5 to drive IFN-γ production and activation of human dendritic cells. *J. Immunol.* 192: 5660–5670.
50. Byrd, A., S. C. Hoffmann, M. Jarahian, F. Momburg, and C. Watzl. 2007. Expression analysis of the ligands for the Natural Killer cell receptors NKp30 and NKp44. *PLoS One* 2: e1339.
51. Tremblay-McLean, A., S. Coenraads, Z. Kiani, F. P. Dupuy, and N. F. Bernard. 2019. Expression of ligands for activating natural killer cell receptors on cell lines commonly used to assess natural killer cell function. *BMC Immunol.* 20: 8.
52. Raulet, D. H., S. Gasser, B. G. Gowen, W. Deng, and H. Jung. 2013. Regulation of ligands for the NKG2D activating receptor. *Annu. Rev. Immunol.* 31: 413–441.
53. Roda-Navarro, P., and H. T. Reyburn. 2009. The traffic of the NKG2D/Dap10 receptor complex during natural killer (NK) cell activation. *J. Biol. Chem.* 284: 16463–16472.